Nuclear Instruments and Methods in Physics Research A 1061 (2024) 169102

Contents lists available at ScienceDirect

Nuclear Inst. and Methods in Physics Research, A

journal homepage: www.elsevier.com/locate/nima

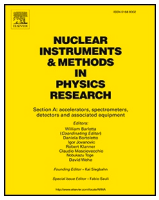

Prediction of JTE breakdown performance in SiC PiN diode radiation detectors using TCAD augmented machine learning

Lan Lin [a,*], Xiu-ku Wang [b], Jian Hu [a]

[a] School of Computer Science and Engineering, Southwest Minzu University, Chengdu, 610041, China
[b] Spallation Neutron Source Science Center, Institute of High Energy Physics, Chinese Academy of Sciences, Dongguan, 523803, China

ARTICLE INFO

Keywords:
SiC
TCAD
Radiation detector
Machine learning
Neural network
Breakdown performance

ABSTRACT

The design of Junction Termination Extension (JTE) is an important step for meeting the reliability requirement of SiC PiN diode radiation detectors. For early evaluation, Technology Computer Aided Design (TCAD) software is often used to simulate the electronic property of detectors with different JTE parameters. But it is time consuming, which need 1 h or even longer for one case. Here, a TCAD augmented Machine Learning (ML) method based on the fully connected Neural Network (NN) algorithm is proposed to predict the breakdown performance quickly with different parameters of Spatial Modulation (SM) JTE. Utilized ~5000 datum generated by TCAD simulation, the ML model could be established and achieve good prediction of breakdown voltage and location within a few seconds. As a semi-supervised learning model, its prediction accuracy of breakdown location is higher than 89.4 % and the determination coefficient R^2 of breakdown voltage could be up to 0.97 compared with TCAD simulations. Moreover, this model could give the relationship curve of breakdown voltages and doping concentration, which is useful to choose an ideal structure with a wide implantation dose window. Based on this ML prediction model, the design cycle of SiC PiN diode radiation detectors could be reduced significantly.

1. Introduction

Compared with silicon, silicon carbide (SiC) as a wide bandgap semiconductor has significantly radiation hardness and the thermal resistance. Based on above properties, SiC has amazing properties for the detection of radiation particles [1–3]. For the detection of charged particles, once they enter the sensitive region of the SiC PiN detectors, many electron-hole pairs will be created. These pairs will drift towards the electrodes under an electric field, and be generated pulse signals. By collecting and analyzing these pulse signals, the detection of incident particles can be achieved. Of course, the wide bandgap characteristics will result in a reduction in the amplitude of the detector's output electrical signal. Usually, SiC PiN diode radiation detectors work on bias voltage. In this case, the termination techniques are often designed to improve breakdown performance of detectors. To guide the design process of JTE and evaluate its breakdown performance early, TCAD simulations are used traditionally [4,5]. But the simulations are time consuming, which would take hours to days when various design constraints. It is greatly delaying the design cycle of radiation detectors. In order to deal with this problem, a novel method is necessary to accelerate the evaluation and design process. It is widely believed that the TCAD augmented machine learning method [6–12] is a good candidate to solve this problem.

Recent years, the TCAD augmented machine learning techniques have been widely used to obtain the inner correlations between the electric performance and the device structure with high accuracy and efficiency [13–17]. This capability provides great assistance for early-stage design, which could obtain an optimize device structure within a short design cycle. As typical representatives, Jing Chen et al. [8] proposed a breakdown performance prediction framework with deep neural networks for SOI lateral power devices. Their results displayed that the accuracy of breakdown location prediction was 97.67 % and the average error of the breakdown voltage prediction was less than 4 % compared with TCAD simulation. Mehta K. et al. [11] demonstrated the possibility to predict full transistor current-voltage and capacitance-voltage curves using Autoencoder trained by TCAD simulation data. Ideal results could be get even with <50 training datum. These literatures verified that ML methods had great potential in optimizing the device structure, and the run time of ML prediction models is efficiency.

* Corresponding author.
E-mail address: linlan0921@163.com (L. Lin).

https://doi.org/10.1016/j.nima.2024.169102
Received 28 July 2023; Received in revised form 19 December 2023; Accepted 10 January 2024
Available online 11 January 2024

Here, we propose a novel prediction model based on the fully connected neural network, which can obtain both the breakdown position and breakdown voltage parameters simultaneously. Compared with the PowerNet model developed by Chen Jing et al. [8], the prediction model mentioned in this paper has a simpler software framework, but the prediction accuracy is equivalent to that of the PowerNet model. Compared to Auto-encoder, the fully connect NN has better self-learning ability, and the number of neurons in the input layer and output layer of a neural network does not have to be the same. Based on the new model, we could quickly obtain the breakdown voltage with R^2>0.97 and determine the breakdown location with 89.4 % accuracy in 1–2 s. Moreover, the ML model could provide the relationship of breakdown voltages and doping concentration, which is easy to choose an ideal structure with a wide implantation dose window. By using this ML model, the design cycle of SiC detectors can be significantly reduced. The scope of application for this predictive model is not confined to the detector structure described in this paper, it can also be extended to other power devices using the SM-JTE terminal structure. The methods employed in this model hold certain reference significance for the rapid establishment of prediction models for breakdown characteristics in SiC devices with alternative terminal structures. It is useful to improve the device yield.

2. TCAD simulation and datasets discussion

As a good candidate to relieve the crowding of the electric field at the corner of the p–n junction, the SM - JTE has been paid much attention in recent years [18–20]. Here, this kind of JTE structure is adopted. Fig. 1 shows a representative 3-D SiC PiN diode radiation detector with SM-JTE and its cross-section along the *A-A'* direction. The doping and thickness of the epi-layer are 2×10^{14} cm^{-3} and 90 μm, separately. In the JTE region, there are 11 annular structures of ion implantation areas. The width of the ith ion implantation area is represented by w_i. The gap between adjacent ion implantation is presented by s, and the width of the gap adjacent to the ith ion implantation area is represented by s_i. The sum of the width of adjacent ion implantation area and gap is represented by M, and $\alpha = w_{i+1}$. Here, the ion implantation concentration is the same in each ion implantation area, represented by N_p. Based on experience, we name the possible breakdown locations as ***zone 1***, ***zone 2***, … …, ***zone n*** ($n \leq 11$). The width of every zone is equal to M.

Based on the Synopsys Sentaurus software, a 2-D simulation model of the SiC PiN diode radiation detector has been constructed. The simulation model includes the mobility model, the recombination generation model, the carrier fermi statistical model which takes into account the Band Gap Narrowing, the incomplete ionization model, and the effective state concentration model based on OldSlotboom. Among them, the mobility model takes into account the effects of temperature (Temperature Dependent) and doping concentration (Doping Dependent), as well as the saturation of mobility under high electric fields. The recombination generation model considers SRH model, Auger model, and Okuto-Crowell's avalanche breakdown model. Because anisotropy has little effect on the breakdown characteristics of devices, in order to improve convergence, the simulation process did not consider anisotropy. Regarding the model parameter settings, the electron mobility is 900 cm^2 V^{-1}•s^{-1} and the hole mobility is 70 cm^2 V^{-1}•s^{-1}. The carrier lifetimes of electrons and holes are 1 μs Other model parameters use the default values. And these parameters, summarized in Table 1, are used for predicting the breakdown voltages and breakdown locations in our ML model.

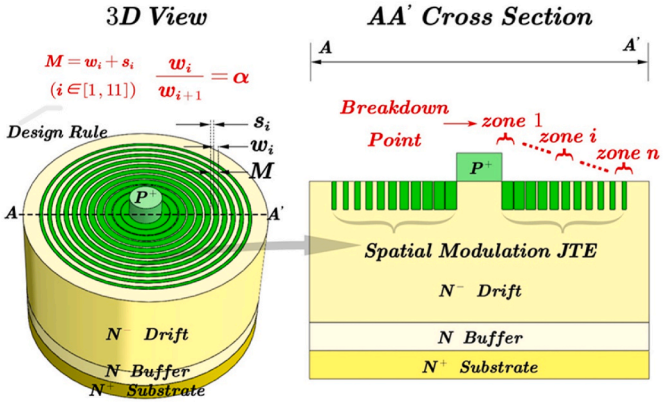

Fig. 1. 3-D SiC PiN diode radiation detector with a circular layout and its cross section along the A-A′ direction.

During these simulations, the cylindrical symmetry is applicated. Grid refinement is set at the main junction position, and additionally grid refinement based on doping concentration gradient rules is set in the terminal implantation zone. The minimal grid size is 0.01 μm. In addition, the specifications of the hardware utilized in this paper are as follows: CPU - Intel(R) Core(TM) i7-8559U @ 2.7 GHz, 8 cores, RAM - 32 GB.

By adjusting the values of α, M and N_p, different breakdown voltages and critical electric fields can be obtained. In this paper, ~5000 TCAD simulation results are used as dataset for machine learning. The relationship between breakdown voltage and M, N_p is shown in Fig. 2.

As is well known, the production of electron-hole pairs due to avalanche generation (impact ionization) requires a certain threshold field strength and the possibility of acceleration within wide space charge regions. If the mean free path exceeds the distance necessary to reach kinetic energies above the threshold energy, impact ionization would occur, potentially causing electrical breakdown. The reciprocal of the mean free path is called the ionization coefficient (ε). With these coefficients for electrons and holes, the avalanche generation rate G^{II} can be expressed by formulas [21,22].

$$G^{II} = \varepsilon_n N v_n + \varepsilon_p P v_p \tag{1}$$

$$\varepsilon(F_{ava}) = f(T) F_{ava}^{\gamma} \exp^{-(g(T) * F_{ava})^{-\delta}} \tag{2}$$

In formula (1), ε_n and ε_p present electron and hole ionizing impact coefficient, N and P present electron hole concentration, v_n and v_p are electron and hole movement velocity. In formula (2), $f(T)$, $g(T)$, γ, and δ are larger than zero. Obviously, the ionization coefficient is monotonically increasing in the electrified region (F_{ava}). According to formula (1), AGR is monotonically increasing with the ε. Based on formulas (1) and (2), we can infer that the avalanche generation rate is high in areas with high electric fields, and breakdown occurs first in regions with the highest avalanche generation rate. Therefore, we can determine the breakdown point of the device by simulating the distribution of the avalanche generation rate. In other words, we could calculate AGR to predict the breakdown location in high voltage devices. Moreover, the value of AGR could be simulated by Synopsys Sentaurus software. For an example, when $\alpha = 1.05$, $N_p = 2.6 \times 10^{17}$cm^{-3}, $M = 20$ μm, the maximum value of AGR appears at 60 μm. We could deduce that the breakdown location is in ***zone 3*** (***zone No.*** $= x \div M$, where x represents the X-direction distance). When we set $N_p = 2.6 \times 10^{17}$cm^{-3}, but adjust α and M separately, the relationship between AGR to α, M and N_p is

Table 1
Structural parameters in the drift region.

Structural parameters	Name	Value
t_{p+}	thickness of P+ layer	2 μm
N_{P+}	doping concentration of P+ layer	2×10^{19} cm^{-3}
t_{epi}	thickness of epi-layer	90 μm
N_{epi}	doping concentration of epi-layer	2×10^{14} cm^{-3}
τ_e	carrier lifetime of electrons	1μs
τ_h	carrier lifetime of holes	0.2μs
μ_e	electron mobility	900 cm^2 V^{-1}•s^{-1}
μ_h	hole mobility	70 cm^2 V^{-1}•s^{-1}

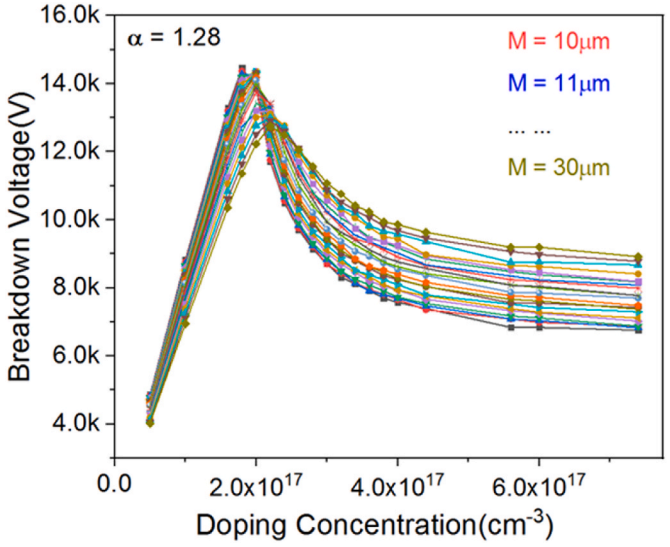

Fig. 2. Relationship between breakdown voltage and doping concentration, when $\boldsymbol{\alpha} = 1.28$, $\boldsymbol{M} = 10$ μm, 11 μm, … …, 30 μm.

shown in Fig. 3.

3. Machine learning model

Here, the fully connected NN algorithm is chosen to predict the JTE breakdown performance in SiC PiN diode radiation detectors, which is running under the TensorFlow framework. We set $\boldsymbol{M}$, $\boldsymbol{\alpha}$, and $\boldsymbol{N_p}$ as the input parameters, and set breakdown voltage and breakdown location as the output results. Schematic diagram of NN based machine learning model is shown in Fig. 4. In the dataset, 66.6 % of them are used for training, and 33.3 % are used for testing. In the dataset, $\boldsymbol{M} \in [10, 30]$, $\boldsymbol{\alpha} \in [1.01, 1.35]$ and $\boldsymbol{N_p} \in [5 \times 10^{16}, 8 \times 10^{17}]$.

In NN algorithm, the number of hidden layers, neurons and epochs would affect the accuracy of output results. Here, mean squared error (MSE) serves as a comprehensive evaluation metric for the two output variables—breakdown voltage and breakdown location. In order to obtain above parameters in the algorithm, we designed some experiments as follow.

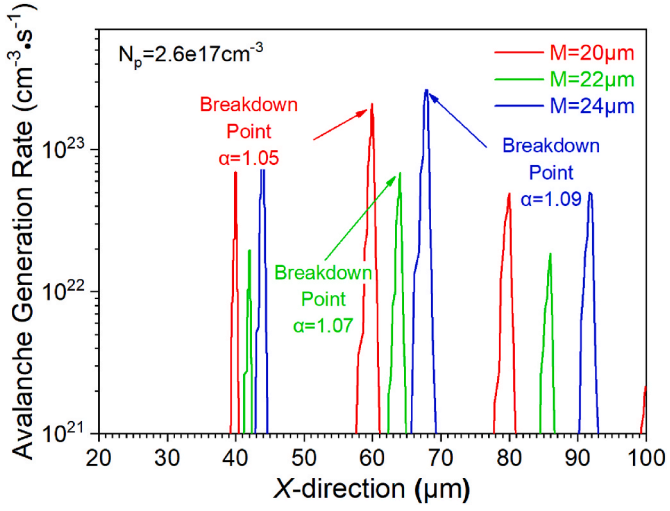

Fig. 3. Relationship between the maximum value of AGR and peak electric fields with different JTE parameters. When $\alpha = 1.05$, $Np = 2.6 \times 10^{17}cm^{-3}$, $M = 20$ μm, the maximum value of AGR appears at 60 μm, which could be deduced that the breakdown location (peak electric field) is in zone 3.

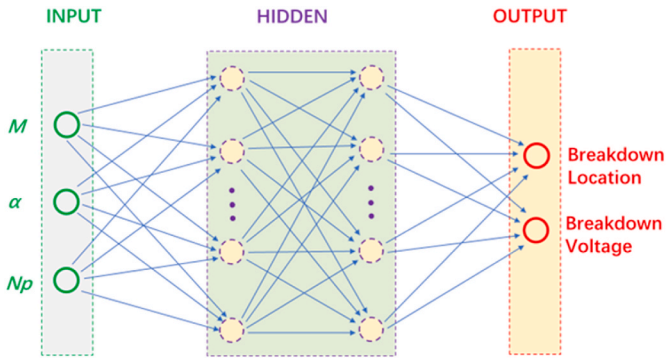

Fig. 4. Schematic diagram of neural network-based machine learning model.

At first, we take the 1st experiment with a fixed number of training epochs at 200. By adjusting the number of hidden layers and the number of neurons, we observe the changes in MSE and obtain the following experimental results as shown in Table 2.

Based on Table 2, we could obtain some information as follow.

1. For 1 hidden layer, its MSE is performed the worst. When the number of neurons is set to 8, the MSE is 5.3E-3. Even with 1024 neurons, the result is 4.7E-4 only.
2. For 2 hidden layers. When the number of neurons is 256, the MSE is up to 3.3E-4.
3. For 3 hidden layers. With 256 neurons, the MSE result is 3.6E-4. This indicates that more hidden layers are not necessarily better. The best performance is achieved with 2 hidden layers.

Next, we carry out the 2nd experiment with a fixed number of training epochs at 200 and a fixed number of hidden layers to 2. By adjusting the number of neurons in each layer, we observe the MSE performance, and the results are shown in Table 3.

As shown in Table 3, when the number of neurons is 256, the MSE is 3.3E-4. However, when the number of neurons is set to 1024, the MSE performs even better, reaching 2.2E-4. Does this mean that the more neurons there are, the better the MSE performance? To test this hypothesis, we design the 3rd experiment, and the results show that the above assumption is incorrect. When the number of training epochs reaches 2000 and the number of neurons is set to 256, the MSE is 1.9E-4. In comparison, when the number of neurons is set to 1024, the MSE is only 2.8E-4. The specific results are shown in Table 4.

Furthermore, we carry out the 4th experiment, in which we keep the number of hidden layers and neurons fixed but vary the number of training iterations. The results are shown in Table 5. It is evident that

Table 2
Fixed Training epochs (200), impact of different number of hidden Layers, and number of neurons on MSE.

Number of neurons in hidden layer 1	Number of neurons in hidden layer 2	Number of neurons in hidden layer 3	MSE
8	–	–	5.3E-3
256	–	–	5.9E-4
1024	–	–	4.7E-4
32	32	–	4.1E-4
256	256	–	3.3E-4
32	32	32	5.0E-4
256	256	256	3.7E-4

Table 3
Fixed numbers of hidden layers and training epochs (200), impact of different number of neurons on MSE.

Number of neurons in hidden layer 1	Number of neurons in hidden layer 2	MSE
8	8	8.9E-4
16	16	6.0E-4
32	32	4.1E-4
64	64	3.8E-4
128	128	3.7E-4
256	256	3.3E-4
512	512	2.9E-4
1024	1024	2.2E-4

Table 4
Fixed numbers of hidden layers and training epochs (2000), impact of different number of neurons on MSE.

Epochs	Number of neurons in hidden layer 1	Number of neurons in hidden layer 2	MSE
2000	256	256	1.9E-4
2000	1024	1024	2.8E-4

Table 5
Fixed numbers of hidden layers and neurons, impact of different training epochs on MSE.

Epochs	Number of neurons in hidden layer 1	Number of neurons in hidden layer 2	MSE
200	256	256	3.3E-4
1000	256	256	2.7E-4
2000	256	256	1.9E-4
4000	256	256	4.9E-4
10,000	256	256	4.0E-4

increasing the number of training iterations does not necessarily lead to better performance. The best MSE performance is achieved when the number of training epochs is 2000, with an MSE of 1.9E-4.

Above all, the prediction model based on the fully connected NN algorithm has 2 hidden layers which contain 256 neurons, and would train 2000 epochs every time. Using the well-trained model, the run time of a prediction experiment with different parameters is only 1–2 s.

4. Results and discussion

Focusing on breakdown voltages and breakdown locations, we carry out two kinds of experiments to compare the ML prediction results with TCAD simulation results. For 1st experiment, the parameters $\boldsymbol{M}$, $\boldsymbol{\alpha}$ and $\boldsymbol{N_p}$ are not in the range of training set, but in the range of dataset. The comparison of the breakdown performance could be shown in Fig. 5, Fig. 6 and Fig. 7. For 2nd experiment, the parameters $\boldsymbol{M'} = 31$, $\boldsymbol{\alpha'} = 1.36$ are not in the range of dataset, but $\boldsymbol{N_p}$ is still in the range $5 \times 10^{16}\text{cm}^{-3}$ to $8 \times 10^{17}\text{cm}^{-3}$. This comparison of the breakdown performance could be seen in Fig. 8 and Fig. 9.

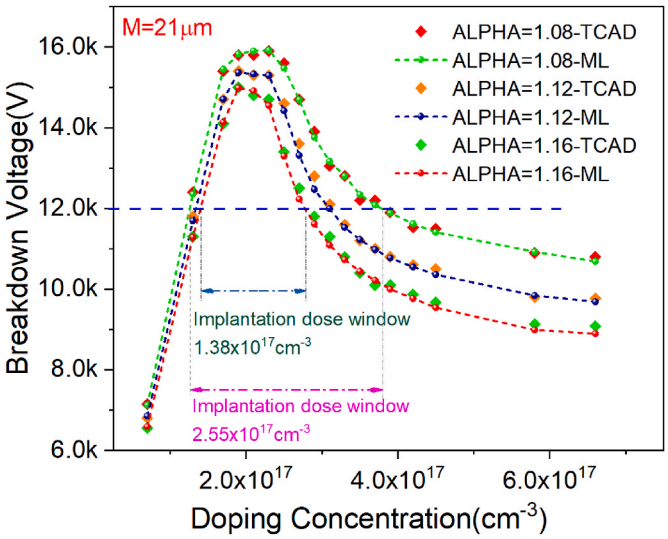

Fig. 5. Prediction results of breakdown voltage with various doping concentration using ML model compared with TCAD simulator. The parameters $\boldsymbol{M}$, $\boldsymbol{\alpha}$ and $\boldsymbol{N_p}$ are not in the range of training set, but in the range of dataset. Scatter points represent TCAD simulation results and dashed lines represent ML prediction results.

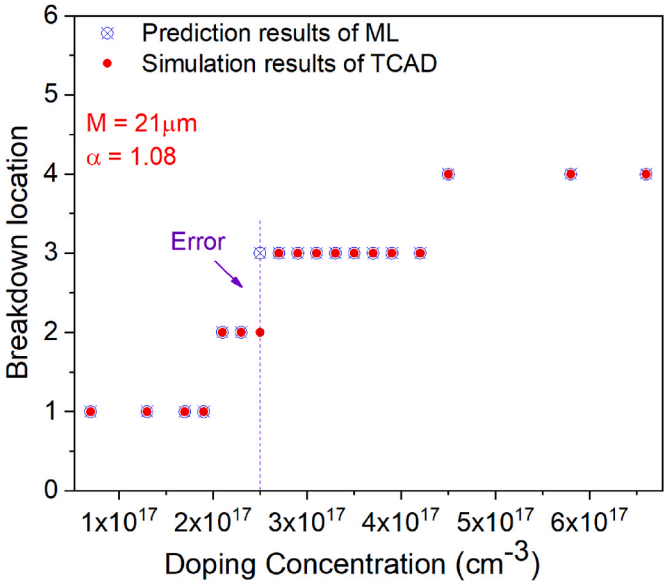

Fig. 6. Prediction results of breakdown location with various doping concentration using ML model compared with TCAD simulator. The parameters $\boldsymbol{M}$, $\boldsymbol{\alpha}$ and $\boldsymbol{N_p}$ are not in the range of training set, but in the range of dataset.

Fig. 5 gives an example showing that the breakdown voltage changes sharply as the doping concentration changes between $7 \times 10^{16}\text{cm}^{-3}$ to $7 \times 10^{17}\text{cm}^{-3}$, which tends to happen in the manufacturing process. Such drastic changes are easily accompanied by many parameters, such as $\boldsymbol{M}$ or $\boldsymbol{\alpha}$. The dots obtained by TCAD simulator are in good agreement with the ML prediction model. When the parameters $\boldsymbol{M} = 21$ μm and $\boldsymbol{\alpha} = 1.08$, the determination coefficient is up to $\boldsymbol{R^2} = 0.99$.

In Fig. 5, we could deduce much more information from the curves obtained by ML model. For an example, when we design a PiN diode radiation detector that withstand voltage is 12 kV. There are many structures could meet the requirement. If we set $\boldsymbol{M} = 21$ μm, $\boldsymbol{\alpha} = 1.08$, the implantation dose window is about $2.55 \times 10^{17}\text{cm}^{-3}$. However, the implantation dose window is only $1.38 \times 10^{17}\text{cm}^{-3}$ when we set $\boldsymbol{\alpha} = 1.16$. Based on this method, it is easy to choose an ideal structure with a

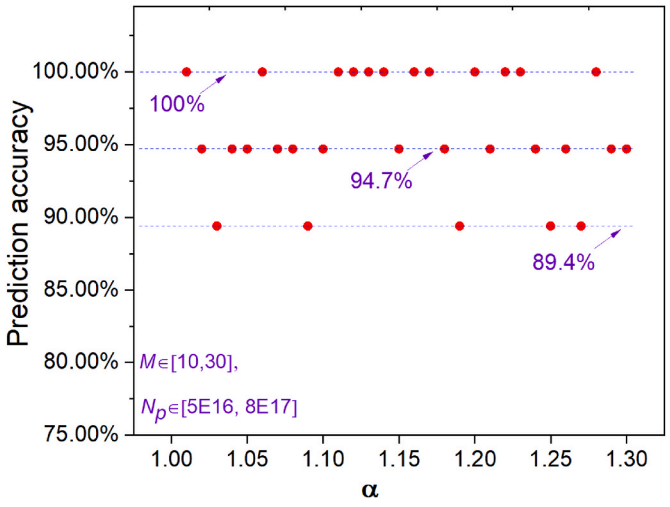

Fig. 7. Prediction results of the breakdown location using the ML model are compared with those from the TCAD simulator. $\boldsymbol{\alpha}\in[1.01, 1.35]$, $\boldsymbol{M} \in [10, 30]$, $\boldsymbol{N_p} \in [5 \times 10^{16}, 8 \times 10^{17}]$. The lowest accuracy recorded at 89.4 %.

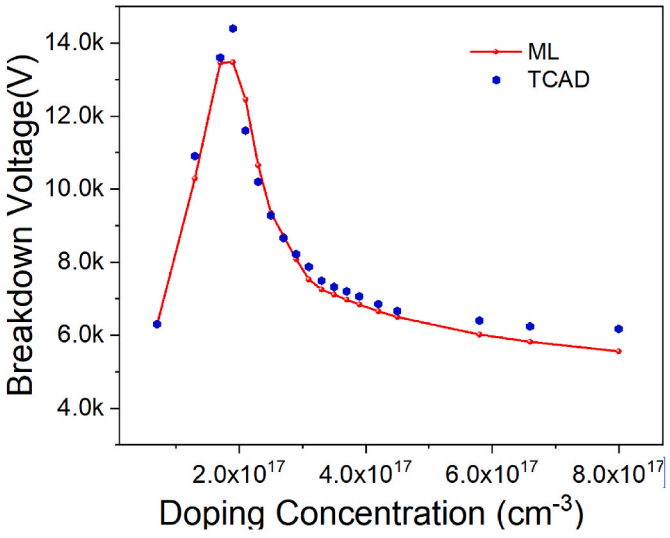

Fig. 8. Prediction results of breakdown voltage with various doping concentration using ML model compared with TCAD simulator. Here, $\boldsymbol{M'} = 31$, $\boldsymbol{\alpha'} = 1.36$, $\boldsymbol{N_p} \in [5 \times 10^{16}, 8 \times 10^{17}]$.

wide implantation dose window, and it is useful to improve the device yield.

The comparison results of breakdown locations with various drift regions doping concentration using ML and TCAD simulator are shown in Fig. 6. When $\boldsymbol{M} = 21$ μm, $\boldsymbol{\alpha} = 1.08$, the use of, ML model allows the accuracy of breakdown location prediction to be as high as 94.7 %.

In this paper, we first set the value of $\boldsymbol{\alpha}$ (such as $\boldsymbol{\alpha} = 1.1$) and then vary the values of $\boldsymbol{M}$ and $\boldsymbol{N_p}$ within a certain range. After running the ML prediction model, we obtain a series of prediction results regarding the breakdown location with $\boldsymbol{\alpha} = 1.1$. These results are then compared with the TCAD simulation results. If they match, the prediction is considered correct; if they differ, the prediction is deemed incorrect. Each solid point in Fig. 7 represents the accuracy of a set of prediction results corresponding to different values of α. Here, $\boldsymbol{\alpha}\in[1.01, 1.35]$, $\boldsymbol{M} \in [10, 30]$, $\boldsymbol{N_p} \in [5 \times 10^{16}, 8 \times 10^{17}]$. When we set the value of $\alpha = 1.1$, the prediction accuracy is 94.7 %. As shown in Fig. 7, the lowest accuracy records at 89.4 %.

In Fig. 8, the comparison results of breakdown voltages between TCAD simulations and ML predictions could be observed when the input

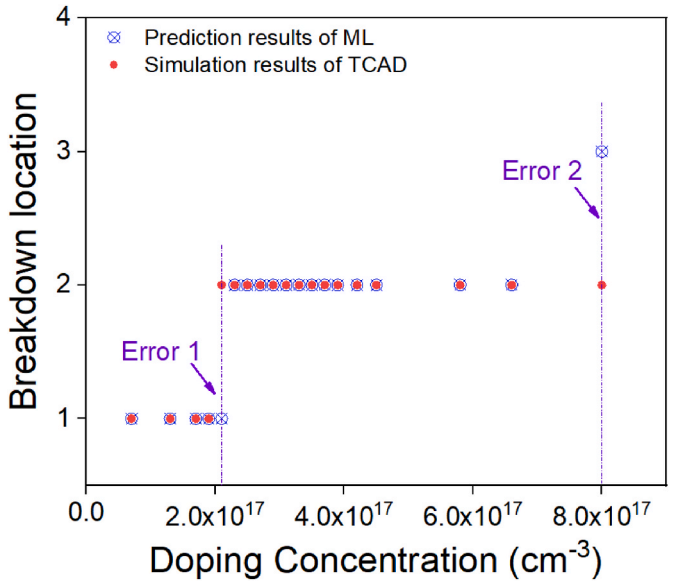

Fig. 9. Prediction results of breakdown location with various doping concentration using ML model compared with TCAD simulator. Here, $\boldsymbol{M'} = 31$, $\boldsymbol{\alpha'} = 1.36$, $\boldsymbol{N_p} \in [5 \times 10^{16}, 8 \times 10^{17}]$.

parameters are set as follow, $\boldsymbol{M'} = 31$, $\boldsymbol{\alpha'} = 1.36$, $\boldsymbol{N_p} \in [5 \times 10^{16}, 8 \times 10^{17}]$. The dots obtained by TCAD simulator are in good agreement with the ML prediction model also. As a semi-supervised learning model, the determination coefficient is up to $\boldsymbol{R^2} = 0.97$, which proves the efficiency of the proposed method.

When $\boldsymbol{M'} = 31$, $\boldsymbol{\alpha'} = 1.36$, $\boldsymbol{N_p} \in [5 \times 10^{16}, 8 \times 10^{17}]$, the comparison results of breakdown locations with various drift regions doping concentration using ML and TCAD simulator are shown in Fig. 9. As a semi-supervised learning model, the accuracy of breakdown location prediction is about 89.4 %.

Based on above comparison experiment results, it still shows good predictive ability. In this case, we can deduce that the use of machine learning for SiC PiN diode radiation detectors design with SM-JTE is a promising direction to move forward. In our opinions, if there is a sufficient training dataset, this model could predict the breakdown performances corresponding to various JTE structures.

5. Conclusion

In this paper, a novel breakdown performance prediction method used TCAD augmented ML is established. This ML model is based on the fully connected NN algorithm, and used ~5000 datum as dataset. During the training process, the effect of hidden layers, the neurons and the training epochs on the MSE is discussed. The well-trained prediction model could predict breakdown location and breakdown voltage efficiently with different parameter of SM-JTE in SiC PiN diode radiation detectors, its run time is about 1–2 s for one case. The prediction accuracy of breakdown location is higher than 89.4 % and the determination coefficient $\boldsymbol{R^2}$ of breakdown voltage could be up to 0.97 compared with TCAD simulator. Further, the ML model could provide the breakdown voltages curve changed along with doping concentration, which is easy to choose an ideal structure with a wide implantation dose window. By utilizing this ML model, the design cycle of SiC PiN diode radiation detectors can be significantly reduced.

CRediT authorship contribution statement

Lan Lin: Funding acquisition, Writing – original draft. **Xiu-ku Wang:** Software. **Jian Hu:** Validation.

Declaration of competing interest

The authors declare that they have no known competing financial interests or personal relationships that could have appeared to influence the work reported in this paper.

Data availability

Data will be made available on request.

Acknowledgment

This research was funded by the Southwest Minzu University Research Startup Funds, China under grant number RQD2021088, the Fundamental Research Funds for the Central Universities-Southwest Minzu University, China under grant number 2021NQNCZ10 and the State Key Laboratory of Nuclear Physics and Technology-Peking University, China under grant number NPT2020KFY16. The authors thank Lin Zhang of Microsystem and Terahertz Research Center, CAEP, for his kind help in TCAD simulation and data analysis.

References

[1] F. Nava, E. Vittone, P. Vanni, et al., Radiation tolerance of epitaxial silicon carbide detectors for electrons, protons and gamma-rays, Nucl. Instrum. Methods Phys. Res. Sect. A Accel. Spectrom. Detect. Assoc. Equip. 505 (3) (2003) 645–655, https://doi.org/10.1016/S0168-9002(02)01558-9.

[2] D. Szalkai, R. Ferone, F. Issa, et al., Fast neutron detection with 4H-SiC based diode detector up to 500 °C ambient temperature, IEEE Trans. Nucl. Sci. 63 (3) (2016) 1491–1498, https://doi.org/10.1109/TNS.2016.2522921.

[3] L.Y. Liu, L. Wang, P. Jin, et al., The fabrication and characterization of Ni/4H-SiC Schottky diode radiation detectors with a sensitive area of up to 4 cm2, Sensors 17 (10) (2017) 2334, https://doi.org/10.3390/s17102334.

[4] L. Zhang, Y.H. Meng, J.T. Li, et al., Fabrication of a 4H-SiC pin diode array for high energy particle detection, IEEE Trans. Nucl. Sci. 69 (9) (2022) 2103–2107, https://doi.org/10.1109/TNS.2022.3194274.

[5] D. Johannesson, M. Nawaz, H.P. Nee, TCAD Model Calibration of High Voltage 4h-SiC Bipolar Junction transistors[C]//Materials Science Forum, vol. 963, Trans Tech Publications Ltd, 2019, pp. 670–673, https://doi.org/10.4028/www.scientific.net/MSF.963.670.

[6] C. Jeong, S. Myung, I. Huh, et al., Bridging TCAD and AI: its application to semiconductor design, IEEE Trans. Electron. Dev. 68 (11) (2021) 5364–5371, https://doi.org/10.1109/TED.2021.3093844.

[7] J. Chen, M.B. Alawieh, Y. Lin, et al., Automatic selection of structure parameters of silicon on insulator lateral power device using Bayesian optimization, IEEE Electron. Device Lett. 41 (9) (2020) 1288–1291, https://doi.org/10.1109/LED.2020.3013571.

[8] J. Chen, M.B. Alawieh, Y. Lin, et al., Powernet: SOI lateral power device breakdown prediction with deep neural networks, IEEE Access 8 (2020) 25372–25382, https://doi.org/10.1109/ACCESS.2020.2970966.

[9] R. Ghoshhajra, K. Biswas, A. Sarkar, A Review on Machine Learning Approaches for Predicting the Effect of Device Parameters on Performance of Nanoscale MOSFETs [J]. *2021 Devices For Integrated Circuit*, DevIC, 2021, pp. 489–493, https://doi.org/10.1109/DevIC50843.2021.9455840.

[10] T. Hirtz, S. Huurman, H. Tian, et al., Framework for TCAD augmented machine learning on multi-I–V characteristics using convolutional neural network and multiprocessing, J. Semiconduct. 42 (12) (2021) 124101, https://doi.org/10.1088/1674-4926/42/12/124101.

[11] K. Mehta, H.Y. Wong, Prediction of FinFET current-voltage and capacitance-voltage curves using machine learning with autoencoder, IEEE Electron. Device Lett. 42 (2) (2020) 136–139, https://doi.org/10.1109/LED.2020.3045064.

[12] H. Dhillon, K. Mehta, M. Xiao, et al., TCAD-augmented machine learning with and without domain expertise, IEEE Trans. Electron. Dev. 68 (11) (2021) 5498–5503, https://doi.org/10.1109/TED.2021.3073378.

[13] M.B. Alawieh, Y. Lin, Z. Zhang, et al., GAN-SRAF: subresolution assist feature generation using generative adversarial networks, IEEE Trans. Comput. Aided Des. Integrated Circ. Syst. 40 (2) (2020) 373–385, https://doi.org/10.1109/TCAD.2020.2995338.

[14] X. Zeng, Z. Li, W. Gao, et al., A novel virtual sensing with artificial neural network and K-means clustering for IGBT current measuring, IEEE Trans. Ind. Electron. 65 (9) (2018) 7343–7352, https://doi.org/10.1109/TIE.2018.2793196.

[15] S.H. Ali, M. Heydarzadeh, S. Dusmez, et al., Lifetime estimation of discrete IGBT devices based on Gaussian process, IEEE Trans. Ind. Appl. 54 (1) (2017) 395–403, https://doi.org/10.1109/TIA.2017.2753722.

[16] H. Carrillo-Nuñez, N. Dimitrova, A. Asenov, et al., Machine learning approach for predicting the effect of statistical variability in Si junctionless nanowire transistors, IEEE Electron. Device Lett. 40 (9) (2019) 1366–1369, https://doi.org/10.1109/LED.2019.2931839.

[17] W. Li, C. Zhang, W. Gao, et al., Neural network self-tuning control for a piezoelectric actuator, Sensors 20 (12) (2020) 3342, https://doi.org/10.3390/s20123342.

[18] G. Feng, J. Suda, T. Kimoto, Space-modulated junction termination extension for ultrahigh-voltage pin diodes in 4H-SiC, IEEE Trans. Electron. Dev. 59 (2) (2011) 414–418, https://doi.org/10.1109/TED.2011.2175486.

[19] T. Yang, S. Bai, R. Huang, Optimization of junction termination extension for ultrahigh voltage 4H-SiC planar power devices, J. Semiconduct. 38 (4) (2017) 044004, https://doi.org/10.1088/1674-4926/38/4/044004.

[20] H. Niwa, G. Feng, J. Suda, et al., Breakdown characteristics of 12–20 kV-class 4H-SiC PiN diodes with improved junction termination structures[C], in: 2012 24th International Symposium on Power Semiconductor Devices and ICs, IEEE, 2012, pp. 381–384, https://doi.org/10.1109/ISPSD.2012.6229101.

[21] F.L.L. Nouketcha, Y. Cui, A. Lelis, et al., Investigation of wide-and ultrawide-bandgap semiconductors from impact-ionization coefficients, IEEE Trans. Electron. Dev. 67 (10) (2020) 3999–4005, https://doi.org/10.1109/TED.2020.3009622.

[22] Sentaurus Device User Guide. 2015. 6, 434.